3D model of laser treatment by a moving heat source with general distribution of energy in the beam

Veselý Zdeněk,[1,*] Honner Milan,[1] and Mach Jiří[2]

[1]New Technologies—Research Centre, University of West Bohemia, Univerzitní 8, Pilsen, 306 14, Czech Republic
[2]University of West Bohemia, Univerzitní 8, Pilsen, 306 14, Czech Republic
*Corresponding author: zvesely@ntc.zcu.cz

Received 30 June 2016; revised 3 October 2016; accepted 3 October 2016; posted 4 October 2016 (Doc. ID 269648); published 0 MONTH 0000

A three-dimensional model of direct heat treatment of a sample surface with a moving laser has been established utilizing the finite element method. Attention is devoted to the preparation of complex boundary conditions of a moving heat source. Boundary conditions of material heat treatment are defined in the form of the heat transfer coefficient with consideration of several effects. Those include general distribution of energy in the laser beam, laser motion velocity, laser axis position outside the sample, and utilization of multiple laser motion tracks over the sample. Various arrangements of sample heat treatment are proposed and computer simulated. Different velocities of laser motion, multiple motion over the same track, and simple motion over a number of tracks are investigated. The temperature distribution in the sample and the depths of material heat treatment are evaluated. The simulation model can be used for temperature prediction during laser surface treatment of materials.

OCIS codes: (000.3860) Mathematical methods in physics; (120.6780) Temperature; (140.3390) Laser materials processing; (140.6810) Thermal effects; (160.3900) Metals; (350.3390) Laser materials processing.

http://dx.doi.org/10.1364/AO.99.099999

1. INTRODUCTION

Laser beams are usually used for surface heat treatment. A laser beam with a certain diameter moves over the surface in proposed tracks to influence the whole surface of the chosen region.

The laser beam is partly reflected; the rest is absorbed to a small depth that is dependent on the absorption coefficient of the material. In the case of metals, the surface absorption of heat power can be assumed.

The application of material heating using a moving heat source has attracted attention for many years. Analytical solutions [1–4] can be obtained under limited conditions. Numerical methods for task solution are used to achieve results for more complex geometries and boundary conditions [5–10].

The authors of [3] deal with an analytical solution of the temperature increase in the material due to stationary/moving bodies. They limit their studies to half-space and half-plane geometries and the integral and differential equations are derived. In [4], the authors utilize an analytical solution for a simple geometrical arrangement.

Numerical simulation of heat transfer in a sample caused by a moving heat source is described in [5]. It considers planar sample geometry, all heat losses to the surroundings are ignored and an ideal heat source with a Gaussian shape is used. The exemplary results include only temperatures in the heat source axis of the trajectory for various velocities of heat source motion.

The authors of [6] deal with heat transfer in a sample with a moving heat source and try to determine the size of the melt area at the sample surface. They consider a hyperbolic heat transfer equation and compare the results with a classic diffusion heat transfer equation. The phase change is already solved in the model. Knowledge of the precise thermal properties of the material dependence on temperature is fundamental in these models. These data are not always available, nor is it possible to measure them. This problem is also solved numerically in [7], using the authors' own method based on the finite difference method. The energy distribution in the heat source is Gaussian-shaped, and all of the material properties and boundary conditions are simplified and assumed to be constants. Also, the planar symmetry of the sample is considered.

The authors of [8] also use their own numerical solution of the heat transfer equation based on the finite difference method. Their numerical solution is compared with an analytical one. Unlike the other works, they use the cluster of heat sources that is used to heat the sample material.

An adaptive mesh scheme of the finite element method (FEM) is used in [9] to solve heat conduction in a solid heated by a moving heat source. A mathematical description of the FEM method including the mathematical procedure of the adaptive mesh scheme that is used for mesh refinement in the areas of large gradients is provided. The results obtained show the functionality of the developed model.

The authors of [10] deal with the effect of heat source beam geometry on the temperature distribution in the material that is assumed to be a half-space. The hyper-elliptical geometry of the heat source beam considered covers a wide range of heat source shapes, including elliptical, rectangular with round corners, rectangular, circular, and square. The effects of the heat source speed, aspect ratio, and other factors are investigated using a general solution of a moving point source on a half-space and superposition of the beam shape.

The majority of the authors use a uniform or Gaussian shape of energy distribution in the heat source and some of the authors use sample material in the shape of a half-space or half-plane. In this paper, a general energy distribution in the laser beam is utilized, because it can reflect the real application of laser heat treatment more precisely than widely used uniform or Gaussian energy distributions.

Authors who deal with the solution of problems of heat transfer in a material that is thermally loaded by a moving heat source use several fundamental possibilities of energy distribution in the heat source: (1) uniform, (2) Gaussian, (3) parabolic, and (4) general. The great majority (4/5) of publications use a uniform distribution of energy in the heat source in order to simplify the solution of the heat transfer process. Some of the publications use a Gaussian energy distribution because it is more precise, and can be easily used, especially when the heat transfer is solved by analytical methods. Only a few authors try to compare different energy distributions and they usually utilize both uniform and parabolic distributions. In the available literature, only one publication has been found that uses a general energy distribution in the heat source [11]. The authors use only a mathematical point of view for the solution of the heat transfer process and do not take into account any real application.

This research is focused on a general distribution of energy in the laser beam because that reflects the real applications of laser heat treatment. Real heat treatment applications employ, instead of laser beams with uniform or Gaussian distributions, laser beams whose energy decreases with increasing distance from the axis of the laser beam with a general shape. When optimization of laser heat treatment of material is utilized with respect to more uniform treatment of the material surface, laser beams with a very specific distribution are taken into account (certain value of heat flux in the center of the beam increases toward the edge of the beam and then rapidly decreases near the beam edge).

A two-dimensional numerical simulation model [12] has been developed for heat transfer during coating deposition in the authors' laboratory. Since then, this model has been improved and widely used for modeling of the dynamic behavior of thermal barrier coatings during thermal shocks [13–15]. The model was also compared with the stochastic solution method [16]. Major improvement of the model has been made to enable heat transfer simulation in 3D sample geometry [17,18].

In this paper, a simulation model of material heat treatment using a moving laser beam and considering 3D geometry with respect to a spatial non-homogeneous profile of the laser beam is investigated. Attention is focused on a description of complex boundary conditions. Results of the individual tasks are shown with respect to variable laser motion velocity, the variable number of movements across the sample using the same track, and the case of several tracks over the sample's front surface.

2. SIMULATION MODEL

A. Model Characteristics

Simulation models of 3D direct non-stationary tasks using the finite element method are prepared. A characteristic feature of the task is the complex boundary conditions of the heat-treated sample surface. A computer model of non-stationary heat transfer is created using the commercial computational system Cosmos/M. The model describes heat treatment using a moving laser beam.

The idea is not to develop a new numerical computational system for the solution of heat transfer processes, but to utilize existing commercial computational systems. When non-standard processes (such as material heating using a moving laser beam) are simulated, the aim is to develop and use a mathematical description of complex processes in the simulation model created in the commercial computational system. This is the reason why only mathematical differential equations of diffusion heat transfer with the additional constraint conditions containing initial and boundary conditions are used in the following text. Moreover, the description and preparation of complex boundary conditions of moving laser beam heating are discussed in detail.

The simulation model is created in the commercial computational system Cosmos/M, which is now part of SolidWorks software. The commercial computational system enables the creation of a simulation model of the heat transfer process (to define the geometry of the model, the physical process to be modeled, initial conditions, boundary conditions, material properties, the computational mesh with the types of finite elements, parameters for the simulation, etc.). Then the system provides the numerical solution of the equations and finally, the system has capabilities for evaluation of the results of the simulation.

The energy distribution in the laser beam is not simplified to a uniform or Gaussian distribution as other authors usually use, but the dependence of energy density on the distance from the laser axis can have a general shape. It is described by an independent user-defined curve, as is discussed in Subsection 2.D.

The sample material is assumed to be homogeneous and isotropic; initial temperature is constant in the sample volume. On the front surface of the sample, the boundary condition of heat convection representing the thermal effect of moving beam source heating (q_{bh}) and the boundary condition of radiation cooling (q_{rc}) are used [Fig. 1(a)]. Lateral sample sides are considered thermally isolated; the back side of the sample has the boundary conditions of free convection cooling (q_{cc}) and radiation cooling (q_{rc}), see Fig. 1(a). The simplified

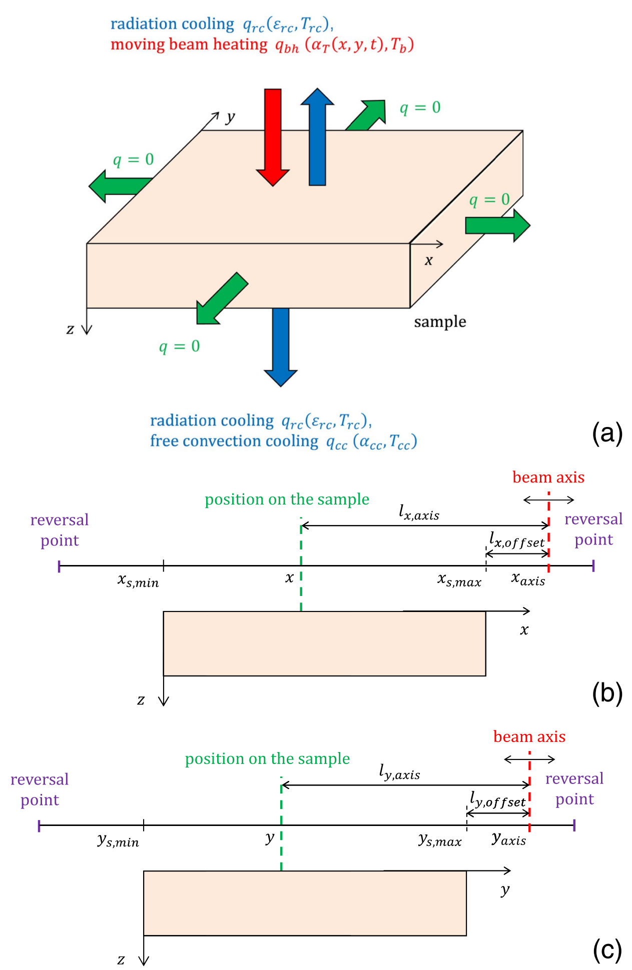

Fig. 1. Scheme of the 3D model of dynamic heat treatment of the sample. (a) Geometry and boundary conditions, heat source motion in the (b) x-axis and (c) y-axis directions.

two-dimensional task is solved in the sample cross section in the xz plane.

The laser beam moves over the sample in certain straight tracks in the x-axis direction [Fig. 1(b)], between the reversal points that are outside the sample. In the simplest case, the beam moves over only one track. When heat treatment fills up the larger surfaces, the beam motion in the y-axis direction [Fig. 1(c)] is made between reversal points outside the sample. The laser beam is circular, with maximum power in the center. Power density declines with increasing distance from the beam axis.

The effect of the moving laser beam is described as a time- and space-dependent surface heat convection on the front sample surface. The basis is the heat transfer coefficient dependence on the distance from the beam axis. The external beam temperature (external temperature for convection) and heat transfer coefficient express heat convection as a boundary condition on the thermally loaded front sample side. The value of external temperature for convection is constant; the heat transfer coefficient is considered to be temperature independent.

Provided that a region of a material heats up above some specific temperature, it is a matter of material heat treatment. When the specific temperature reaches the so-called hardening temperature T_h, and the heating process is followed by rapid cooling of the material, the overall process is called material hardening. The hardening temperature T_h is approximately 800°C. Provided a laser beam is the heating source, it is called surface laser hardening. For surface laser hardening, a high-intensity heat flux in the laser spot is characteristic, which results in very rapid heating of the surface layer of the material and subsequent rapid cooling due to heat transfer further into the material. There is a change of phases and transformation of the surface layer to high hardness due to the rapid cooling of the heated material. Especially the speed of the heating and cooling processes, the formation of a high temperature gradient, and the absence of a liquid cooling medium are three fundamental advantages of this process.

B. Model Mathematical Description

The partial differential equation for diffusion heat transfer in the sample material without inner heat sources has the form

$$\operatorname{div}(\lambda(x,y,z,t)\operatorname{grad} T(x,y,z,t)) = c(x,y,z,t)\rho(x,y,z,t)\frac{\partial T(x,y,z,t)}{\partial t}, \tag{1}$$

where x, y, z are spatial coordinates; t is the time of the process; $T(x,y,z,t)$ is the temperature of the sample; $\lambda(x,y,z,t)$, $c(x,y,z,t)$, and $\rho(x,y,z,t)$ are spatial and time-dependent thermal conductivity, specific heat capacity, and density.

The set of additional constraints involves the initial condition and several types of boundary conditions. The initial condition is in the form

$$T(x,y,z,0) = T_{\text{ini}}(x,y,z), \tag{2}$$

where $T_{\text{ini}}(x,y,z) = T_{\text{ini}}$ is the initial sample temperature that is assumed to be constant for the whole sample volume.

The heat flux boundary condition is in the form

$$-\lambda(x,y,z,t)\frac{\partial T(x,y,z,t)}{\partial \boldsymbol{n}} = \boldsymbol{q}_p(x,y,z,t), \tag{3}$$

where $\boldsymbol{n}$ is the normal vector to the surface in the position x, y, z. Partial derivative $\partial T/\partial \boldsymbol{n}$ expresses the derivative of the temperature in the direction perpendicular to the sample surface. The vector quantity $\boldsymbol{q}_p(x,y,z,t)$ denotes the prescribed value of heat flux at the sample boundary. Boundary conditions of this type are used for lateral sample sides [see Fig. 1(a)]. Prescribed surface heat flux is equal to zero $\boldsymbol{q}_p(x,y,z,t) = 0$.

The convective heat transfer boundary condition is used in the form

$$-\lambda(x,y,z,t)\frac{\partial T(x,y,z,t)}{\partial \boldsymbol{n}} = \alpha_{\text{cc}}(x,y,z,t)(T(x,y,z,t) - T_{\text{cc}}(x,y,z,t)), \tag{4}$$

where $\alpha_{\text{cc}}(x,y,z,t)$ is the prescribed heat transfer coefficient for convection cooling, $T_{\text{cc}}(x,y,z,t)$ is the prescribed external temperature for convection cooling, and $T(x,y,z,t)$ is the sample surface temperature, because the equation is valid only for the positions on the sample boundary. The equation expresses the linear relation between the sample surface temperature and its gradient. A boundary condition of this type is utilized for free convection cooling at the sample back side [Fig. 1(a)].

Convective heat transfer for moving beam heating at the front side of the sample is described using the total heat transfer coefficient $\alpha_T(x, y, z, t)$, computed from Eqs. (8) or (10) and the external temperature, called the laser beam temperature T_b,

$$-\lambda(x, y, z, t)\frac{\partial T(x, y, z, t)}{\partial \boldsymbol{n}} = \alpha_T(x, y, z, t)(T(x, y, z, t) - T_b(x, y, z, t)), \tag{5}$$

where the total heat transfer coefficient $\alpha_T(x, y, z, t)$ is defined so as to include all the sample heating by the moving laser beam, which means both convective and radiative parts of the heating from the laser beam [Fig. 1(a)].

The radiation heat transfer boundary condition has the form

$$-\lambda(x, y, z, t)\frac{\partial T(x, y, z, t)}{\partial \boldsymbol{n}} = \varepsilon_p(x, y, z, t)\sigma_0(T^4(x, y, z, t) - T^4_{\mathrm{rc}}(x, y, z, t)), \tag{6}$$

and expresses the radiative cooling of the sample. The quantity ε_p denotes the prescribed emissivity of the sample surface, σ_0 is the Stefan–Boltzmann constant, and T_{rc} is the external temperature for sample radiation cooling. The prescribed sample surface emissivity is assumed as a constant value, but the model created enables the utilization of a temperature-dependent value of sample surface emissivity. A boundary condition of this type is assumed at front and back sides of the sample for radiation cooling [Fig. 1(a)].

Because the convective heat transfer for moving beam heating is used only on the front side of the sample, where the position $z = 0$ holds, the full expression $\alpha_T(x, y, 0, t)$ is substituted by the simplified form $\alpha_T(x, y, t)$ in the following text.

C. Characteristics of Complex Boundary Conditions

For the computation of time dependence of the *total heat transfer coefficient* α_T for a certain position (certain computational node) on the thermally loaded sample side, it is necessary to know the *basic heat transfer coefficient* α_B dependence on the distance from the beam axis $l_{x,\mathrm{axis}}$ in the x-axis direction, the actual position of the beam axis x_{axis} in the x-axis direction, the actual distance of the beam axis from the sample side $l_{x,\mathrm{offset}}$ in the x-axis direction, the dependence of the *reduction coefficient* $c_{\alpha,x}$ on the distance of the beam axis from the sample side $x_{s,\min}$ (and also $x_{s,\max}$) in the x-axis direction, the distance from the beam axis $l_{y,\mathrm{axis}}$ in the y-axis direction, the actual position of the beam axis y_{axis} in the y-axis direction, the actual distance of the beam axis from the sample side $l_{y,\mathrm{offset}}$ in the y-axis direction, and the dependence of the *reduction coefficient* $c_{\alpha,y}$ on the distance of the beam axis from the sample side $y_{s,\min}$ (and also $y_{s,\max}$) in the y-axis direction.

The value of the basic heat transfer coefficient α_B dependent on the distances from the beam axis $l_{x,\mathrm{axis}}$, and also $l_{y,\mathrm{axis}}$, in the x-axis, and also y-axis, directions represent the real space distribution of beam power. This distribution is assumed to be axially symmetric.

Reduction coefficients $c_{\alpha,x}$, and also $c_{\alpha,y}$, dependent on the distance of the beam axis from the sample side $l_{x,\mathrm{offset}}$, and also $l_{y,\mathrm{offset}}$, in the x-axis, and also y-axis directions on the sample take into account the state when the beam axis is outside the sample. Reduction coefficients are equal to one, when the beam axis is over the sample surface, and decrease with increasing distance of the beam axis from the sample edge.

1. Simple Description of Boundary Conditions for the 3D Model

This approach expresses a simple description of a 3D task. It is used when commercial computation software enables only a limited number of time curves. A simple description of boundary conditions expresses the definition of time curves only for computational nodes on the laser track at the sample surface. The times curves for other nodes at the sample surface are computed from time curves of laser track nodes using the multiplication coefficient called *normalized heat transfer coefficient* α_N. The simple 3D simulation model can be assumed to be an enhancement of the 2D model.

The advantage of this model is a simpler evaluation of boundary conditions and the ability to utilize a small number of times curves. A small disadvantage is the slight disruption of the rotational symmetry of the laser spot.

From the mathematical point of view, the dependence of the *total heat transfer coefficient* α_T on the y-axis is replaced with the *normalized heat transfer coefficient* α_N. The normalized heat transfer coefficient is dependent on the distance from the beam axis in the y-axis direction and the actual position of the beam axis y_{axis} in the y-axis direction.

Characteristic courses of the basic heat transfer coefficient, reduction coefficients, actual positions of the beam axis, and the normalized heat transfer coefficient are schematically illustrated in Fig. 2(a) (input courses for model). The aim is to evaluate the dependence of total heat transfer $\alpha_T(x, y, t)$, see Fig. 2(c). The time dependence of α_T for certain values of x, y (positions on the loaded sample side) defines the heat transfer coefficient for individual computational nodes. These time dependencies for individual nodes can be directly loaded to the computational system during simulation model preparation.

2. Full Description of Boundary Conditions for the 3D Model

This approach gives a full precise description of the 3D task. It is used when the computation software enables a sufficient number of time curves. A full description of boundary conditions consists of the definition of time curves for all sample surface computational nodes.

The advantage is to preserve the rotational symmetry of the laser spot. A small disadvantage is the more complicated evaluation of boundary conditions.

From the mathematical point of view, the *total heat transfer coefficient* α_T is dependent directly on the distance from the axis of the laser beam.

Characteristic courses of the basic heat transfer coefficient, reduction coefficients, and actual positions of the beam axis are schematically illustrated in Fig. 2(b) (input courses for model) and Fig. 2(c) (final output curve). These time dependencies for individual nodes can be directly loaded to the computational system during preparation of the simulation model.

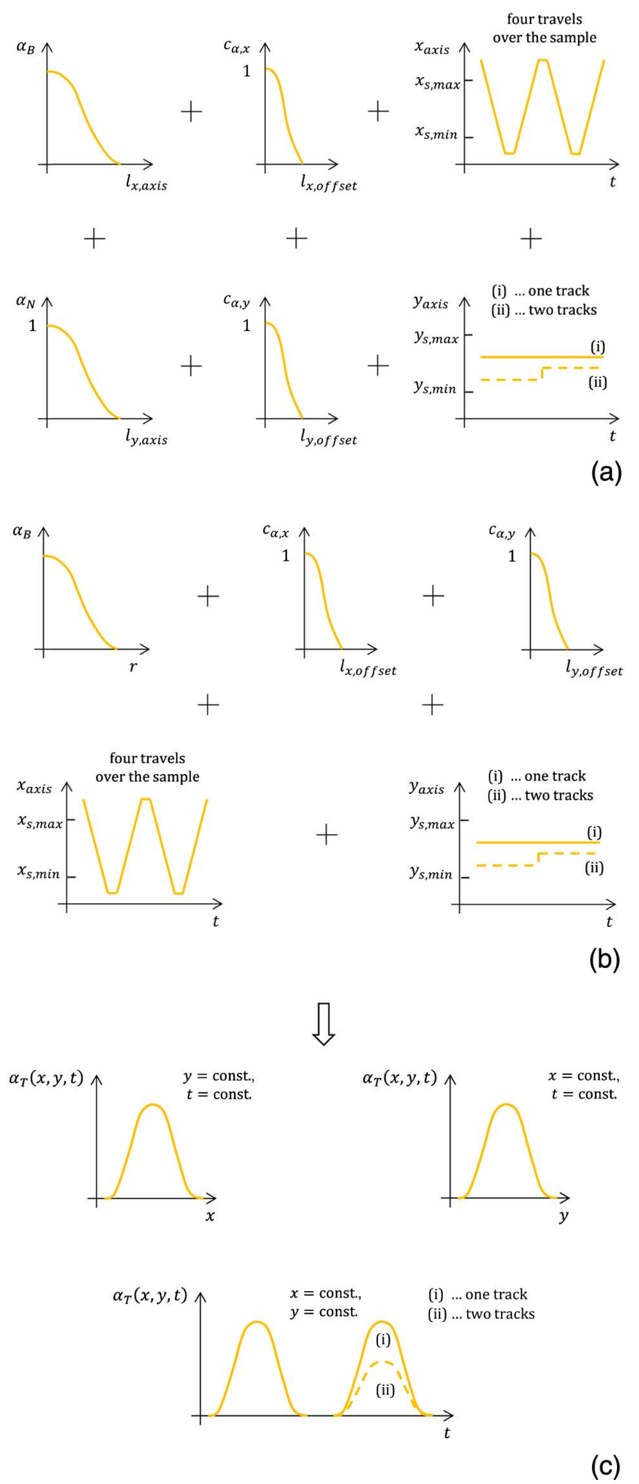

Fig. 2. Scheme of boundary condition preparation using a moving heat source. (a) Input courses of quantities for a simple 3D model, (b) input courses of quantities for a full 3D model, (c) output curve of the total heat transfer coefficient.

D. Mathematical Description of Complex Boundary Conditions

Mathematical equations of boundary conditions for the thermally loaded front side of the sample depend on the simplicity or complexity of their descriptions.

1. Simple Description of Boundary Conditions

The distribution of the total heat transfer coefficient $\alpha_T(x, t)$ in the x-axis direction is determined in Eq. (1). Subsequently, the total heat transfer coefficient of $\alpha_T(x, y, t)$ is evaluated, Eq. (8), by multiplication of $\alpha_T(x, t)$ by the normalized heat transfer coefficient α_N, which describes the attenuation of laser power in the y-axis direction. It is expressed by Eqs. (7–9) and (12–19), and represents a simple description of the 3D task.

2. Full Description of Boundary Conditions

The distribution of the total heat transfer coefficient $\alpha_T(x, y, t)$ in the x- and y-axes directions is determined by Eq. (10). The total heat transfer coefficient depends on the direct distance from the laser spot axis defined by Eq. (11). This is a mathematically precise procedure reflecting the full axis symmetry of the heat transfer coefficient. The full description of boundary conditions is performed using Eqs. (10) and (11), and (12–19).

In this case, the computational software has to enable a sufficient number of time curves so that each computational node at the heat-loaded sample surface has its own time curve of the total heat transfer coefficient:

$$\alpha_T(x, t) = \alpha_B(l_{x,\text{axis}}(x, t))c_{\alpha,x}(l_{x,\text{offset}}(t)), \quad (7)$$

$$\alpha_T(x, y, t) = a_T(x, t)a_N(l_{y,\text{axis}}(y, t))c_{a,y}(l_{y,\text{offset}}(t)), \quad (8)$$

$$\alpha_N(l_{y,\text{axis}}(y, t)) = \alpha_B(l_{y,\text{axis}}(y, t))\alpha_{B,\max}^{-1}, \quad (9)$$

or

$$\alpha_T(x, y, t) = \alpha_B(r(x, y, t))c_{a,x}(l_{y,\text{offset}}(t))c_{a,y}(l_{y,\text{offset}}(t)), \quad (10)$$

$$r(x, y, t) = \sqrt{l_{x,\text{axis}}^2(x, t) + l_{y,\text{axis}}^2(y, t)}, \quad (11)$$

with other quantities defined as

$$l_{x,\text{axis}}(x, t) = |x(t) - x_{\text{axis}}(t)|, \quad (12)$$

$$l_{y,\text{axis}}(y, t) = |y(t) - y_{\text{axis}}(t)|, \quad (13)$$

$$l_{x,\text{offset}}(t) = 0 \ldots x_{s,\min} < x_{\text{axis}}(t) < x_{s,\max}, \quad (14)$$

$$= |x_{s,\min} - x_{\text{axis}}(t)| \ldots x_{\text{axis}}(t) < x_{s,\min}, \quad (15)$$

$$= |x_{s,\max} - x_{\text{axis}}(t)| \ldots x_{\text{axis}}(t) > x_{s,\max}, \quad (16)$$

$$l_{y,\text{offset}}(t) = 0 \ldots y_{s,\min} < y_{\text{axis}}(t) < y_{s,\max}, \quad (17)$$

$$= |y_{s,\min} - y_{\text{axis}}(t)| \ldots y_{\text{axis}}(t) < y_{s,\min}, \quad (18)$$

$$= |y_{s,\max} - y_{\text{axis}}(t)| \ldots y_{\text{axis}}(t) > y_{s,\max}. \quad (19)$$

E. Parameters of the Simulation Model

A laser source with power $P = 4.5$ kW and beam diameter $r_b = 10$ mm is selected for the simulation. The sample is made from steel ČSN 15330 with dimensions 100 × 70 × 20 mm. The sample material properties are assumed to be temperature dependent. The values of the thermal conductivity λ, specific heat capacity c, and density ρ in the selected range from 20°C to 1073°C are shown in Table 1.

Laser beam motion velocities are in the range from 17.15 to 40 mm · s^{-1} and the distances of reversal points of laser tracks

Table 1. Temperature-Dependent Material Properties of Steel Sample ČSN 15330

Temperature T(°C)	Thermal Conductivity λ(W.m^{-1}.K^{-1})	Specific Heat Capacity c(J.kg^{-1}.K^{-1})	Density ρ(kg.m^{-3})
20	40.49	421.3	7821
100	39.77	438.7	7798
200	38.85	474.5	7768
300	37.89	526.0	7737
400	36.90	593.3	7704
500	35.87	676.2	7671
600	34.82	774.9	7636
700	33.73	889.3	7600
800	32.61	1019.4	7563

from the sample edge are 10 mm. The laser beam moves along a track passing over the center of the loaded surface; motion begins at the right reversal point and finishes at the same position. Sample absorptivity a is equal to emissivity ε and emissivity for radiation cooling $\varepsilon_{\mathrm{rc}}$ ($a = \varepsilon = \varepsilon_{\mathrm{rc}} = 0.7$). External temperatures for radiation and convection coolings are equal to sample initial temperature $T_{\mathrm{rc}} = T_{\mathrm{cc}} = T_{\mathrm{ini}} = 20°\mathrm{C}$.

Space distribution of the basic heat transfer coefficient $\alpha_B(r)$ dependent on the distance from the beam axis is assumed according to Fig. 2(a). The quantity course is described by the values $\alpha_B(r) = \alpha_{B,\max}$ for $r = 0$, $\alpha_B(r) = \alpha_{B,\max}/2$ for $r = r_b/2$, and finally $\alpha_B(r) = 0$ for $r = r_b$. For the maximum of the basic heat transfer coefficient, the following holds:

$$P = \varepsilon S_{\mathrm{red}}\, \alpha_{B,\max}(T_b - T_S), \tag{20}$$

where S_{red} is the reduced surface of the laser spot $S_{\mathrm{red}} = \pi r_{\mathrm{red}}^2$, $r_{\mathrm{red}} = r_b/2$, and T_S is the sample surface temperature. Beam temperature T_b is set to a specific value. Absolute values of the basic heat transfer coefficient and specific temperature of the laser beam are linked together and give the value of power P.

Generally, the boundary condition coefficients, such as the emissivity ε and the basic heat transfer coefficient α_{B}, are assumed to be constant in the model. The constant value of the basic heat transfer coefficient corresponds with reality (when the surface does not melt), because the value does not change with the surface temperature nor with the state of the surface. However, the value of the emissivity undergoes small changes during the laser heat treatments even without surface melting. The precise values of the emissivity during the treatment process are not known. Therefore, a constant value of the emissivity is assumed. On the other hand, the simulation model created enables the utilization of temperature-dependent emissivity, if it is known.

F. Simulated Cases of Laser Treatment

Several simulation models have been created in order to compare heat distribution in the sample during various thermal laser processing procedures. A typical technological example of laser surface heat treatment is laser surface hardening [19,20]. Generally, the field of laser material treatment is a continually evolving area [21–23].

- **First simulation case.** A comparison of laser beam motion velocity is provided for three velocities 17.14, 24, and 40 mm · s^{-1} (corresponding to the 7, 5, and 3 s time of motion between opposite reversal points). The two continuous back-and-forth movements of the beam are conducted with the total process times of 14, 10, and 7 s. The computational results are studied to evaluate the effect of various motion velocities on the sample temperatures.

This simulation case is a typical technological case of searching for processing parameters [24–26]. During the process of laser hardening, the laser power is set up and the optimum values of the parameters (e.g., motion velocity of the laser beam) are sought.

- **Second simulation case.** Multiple back-and-forth movements across the sample using the same track are carried out with the motion beam velocity 24 mm · s^{-1} (corresponding to the 5 s motion time between opposite reversal points); the total process time is 20 s. The four movements of the beam use the same track over the sample. The simulation results are compared to evaluate the differences among the various numbers of movements across the sample.

This simulation case corresponds to a real application of the scanning laser hardening method [24–26]. In this real application, there is a very small hatch of individual small laser lines and thus the simulation case is an approximation of the arrangement when zero spacing of laser lines is used and the laser beam moves along the same track repeatedly.

- **Third simulation case.** One movement across multiple tracks is carried out with the motion beam velocity 24 mm · s^{-1} (corresponding to the 5 s motion time between opposite reversal points). The total process time is 17 s, because among the three tracks in the x-axis direction, there are two movements in the y-axis direction that take 1 s each. Each movement of the beam uses a different track over the sample. The simulation results are studied to evaluate the effect of various tracks over the sample on the sample temperatures.

This simulation case is a technological case of surface hardening using a wide laser beam of a continuous laser. The laser beam moves over the surface of the material with a certain spacing of individual lines to gradually apply laser heat treatment on the whole surface of the sample [20,27].

3. RESULTS

Evaluating the results from the simulation models, attention is focused on sample temperature distribution, maximum temperature values at the sample surface, and the depths of the laser heat treatment.

A. Effect of Laser Beam Motion Velocity

The sample temperature distribution dependent on beam motion velocity is observed. Total process times (two movements over the sample) 14, 10, and 7 s correspond to simulated motion velocities 17.14, 24, and 40 mm · s^{-1}. Because the process time depends on motion velocity, the process dimensionless time Θ is introduced, whose values are in the range 0–1 for all cases of beam motion. Dimensionless time $\Theta = 0$ means that the laser beam is at the right reversal point, $\Theta = 0.5$ denotes that the beam reached the left reversal point, and value $\Theta = 1.0$ shows the laser beam to be back at the right reversal point.

Figure 3 illustrates time courses of temperature in the center of the sample front surface and below this position. At

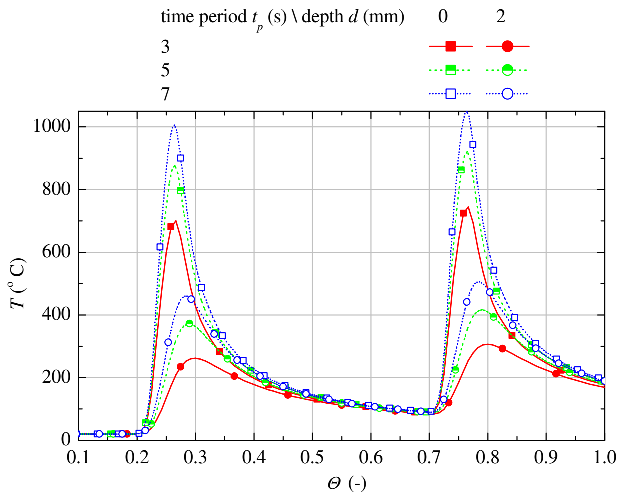

Fig. 3. Time courses of the temperature in the center of the sample front surface for depths 0 and 2 mm ($x = 50$ mm, $y = 35$ mm).

dimensionless times equal to 0.25 and 0.75, the heat source position is over the sample center. Using motion velocity 40 mm · s^{-1}, the surface temperature in the center of the track is 700°C during the first movement of the laser beam and approximately 740°C for the second beam movement. In the case of 24 mm · s^{-1} motion velocity, the surface center temperature has its maximum about 870°C during the first beam movement, and 920°C during the second movement. These temperatures exceed the ones for the material heat treatment. In accordance with expectations, with the lowest motion velocity of 17.14 mm · s^{-1}, the surface center temperature maximum is higher than in the previous case. The surface center temperature maximum is approximately 1000°C for the first, and 1050° C for the second laser beam movement.

Figure 4 shows spatial courses of temperature in the z direction passing the sample center. Dimensionless time is a parameter of temperature curves. At the dimensionless time $\Theta = 0.75$, the heat source is directly under the sample center during the second movement. The velocity value has a great effect on temperature spatial courses. Surface temperatures

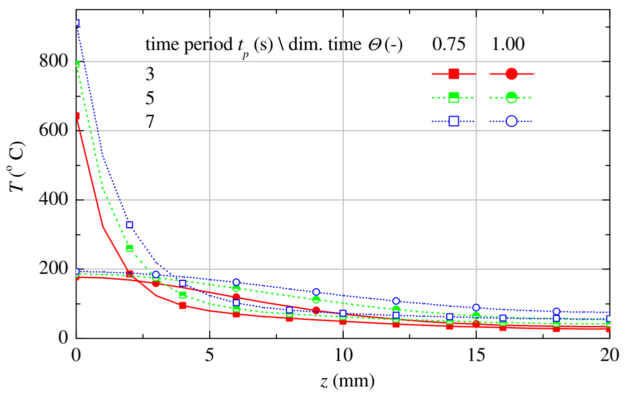

Fig. 4. Spatial courses of the temperature in the z-axis direction passing the center of the sample for dimensionless times 0.75 and 1.0 ($x = 50$ mm, $y = 35$ mm).

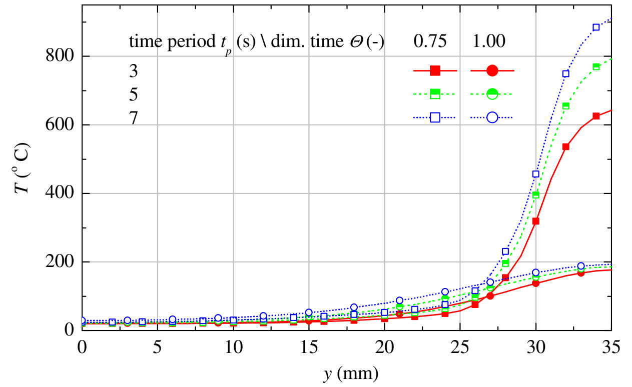

Fig. 5. Spatial courses of the temperature in the y-axis direction passing the center of the sample front surface for dimensionless times 0.75 and 1.0 ($x = 50$ mm, $z = 0$ mm).

are high in the range 650°C–900°C, but they rapidly decrease with depth increase. The temperature is below 200°C at the 3 mm depth. At the dimensionless time $\Theta = 1.0$, the heat source is back at the right reversal point. The depth temperature profile is more balanced than at the time $\Theta = 0.75$. This denotes fast temperature equalization in the sample material. The different beam motion velocity has only a small influence on spatial courses of temperature at dimensionless time $\Theta = 1.0$.

The spatial profile of surface temperature in the direction perpendicular to the beam track is in Fig. 5. The parameter of the curves is dimensionless time again. At the dimensionless time $\Theta = 0.75$, the beam is directly under the sample center during the second movement. The width of the heat-affected zone has only slight differences, but the temperatures obtained in this zone vary for tested motion velocities. At the dimensionless time $\Theta = 1.0$, surface temperature profiles in the y-axis direction gradually flatten, similarly as in the z-axis direction (Fig. 4).

B. Effect of Multiple Movements across the Same Track

The sample temperature during the laser treatment with a number of movements along the same track is described in this section. The laser beam motion velocity is 24 mm · s^{-1}, which corresponds to 5 s of travel time between the opposite reversal points of the track. Four movements are done in total. The time courses of temperature at the center of the sample surface and several positions below are displayed in Fig. 6. During the first movement of the laser beam over the sample, the sample temperature at the center of the track reaches over 800°C. Increasing the number of movements, this temperature slightly increases to nearly 950°C during the fourth movement. Taking the depths of 1 and 2 mm, the maximum temperature at the track center decreases. The temperature of 600°C at the depth of 1 mm is exceeded until the third laser movement.

Figure 7 shows spatial courses of temperature both in the z direction going through the sample center (lower x-axis in the graph, solid line) and in the y-axis direction (higher x-axis in the graph, dotted line). The first two time levels shown are 7.5 and 17.5 s (when the laser is passing through the center of the track

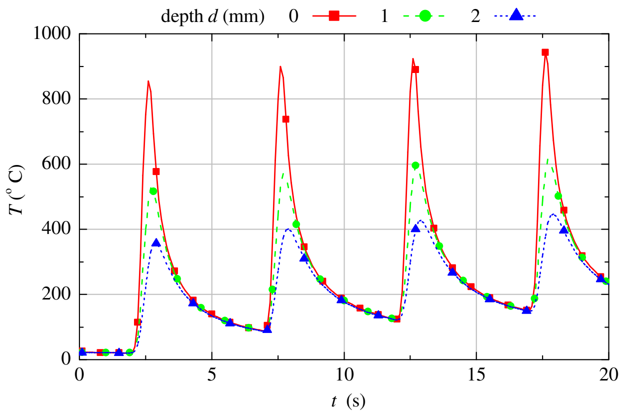

Fig. 6. Time courses of the temperature in the center of the sample front surface for depths from 0 to 2 mm ($x = 50$ mm, $y = 35$ mm).

in the second and fourth movements). The temperature rapidly decreases with increasing depth from the surface. The times when the laser is in the reversal position after the second and fourth movements (10 and 20 s) are characterized by more balanced temperature profiles.

The surface temperature profiles in the y-axis direction (dotted lines in Fig. 7) present the decrease of temperature with increasing distance from the track. At the times of 7.5 and 17.5 s, the width of the heat-affected zone is clearly visible in the figure. When the laser beam is outside the sample, the temperature profiles in the y-axis direction flatten similarly as in the z-axis direction. The maximum surface temperature is about 240°C at the end of the laser treatment.

C. Effect of One Movement across Multiple Tracks

When the laser treatment of a certain area should be done, a number of tracks are used to provide full coverage of this area, and the tracks are separated by some distance. In this section, three tracks in the x-axis direction, each separated by the distance of 20 mm, are used to test the simulation model created.

The laser beam motion starts at the A position (Fig. 8). Each track takes 5 s to travel, while y-axis motions take 1 s. The surface treatment ends when the laser beam reaches the B position.

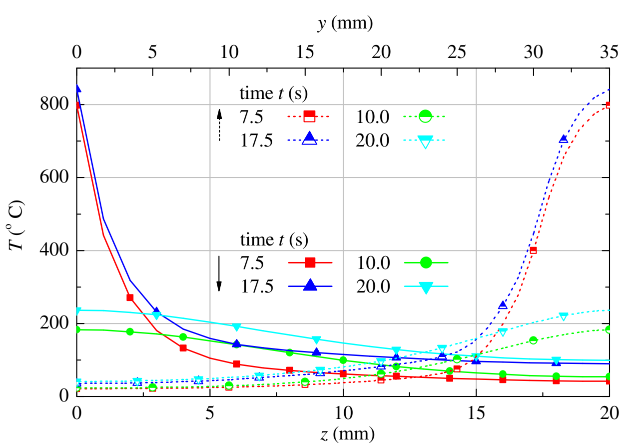

Fig. 7. Spatial courses of the temperature in the z- and y-axes directions passing the center of the sample front surface for selected times ($x = 50$ mm).

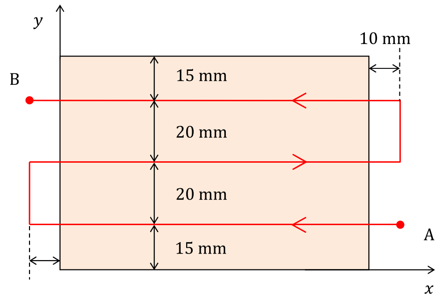

Fig. 8. Scheme of tracks across the sample.

Figure 9 shows time courses of surface and subsurface (depth 1 mm) temperatures in the center of each track. The red line shows the temperatures in the center of the first track. As the laser beam comes to the center of the track, the temperature increases and the maximum value is achieved when the laser spot is a small distance after the center of the track. Then the sample temperature at the track center rapidly decreases and the surface and subsurface (at the depth of 1 mm) temperatures equalize. The temperature courses at the center of tracks II and III have a similar character, only time shifted.

Temperature spatial profiles perpendicular to the laser tracks and passing their centers are shown in Fig. 10. The red line shows the temperature profile at the time 2.5 s, when the laser beam is over the center of track I. The temperature profiles at the times of 8.5 and 14.5 s have similar peaks. The peak values of temperature profiles shown are about 760°C, while their maximum values of approximately 870°C are attained several tenths of a second later.

The distance between the laser tracks in this sample heat treatment is too wide. Considering the temperature curves in Fig. 10, in order to achieve a uniform surface heat treatment, the distance between the laser tracks should be reduced. The temperature profiles in Fig. 10 are for sample surface positions. The temperature profiles at subsurface positions would have a similar trend, but distinctly lower values of temperature.

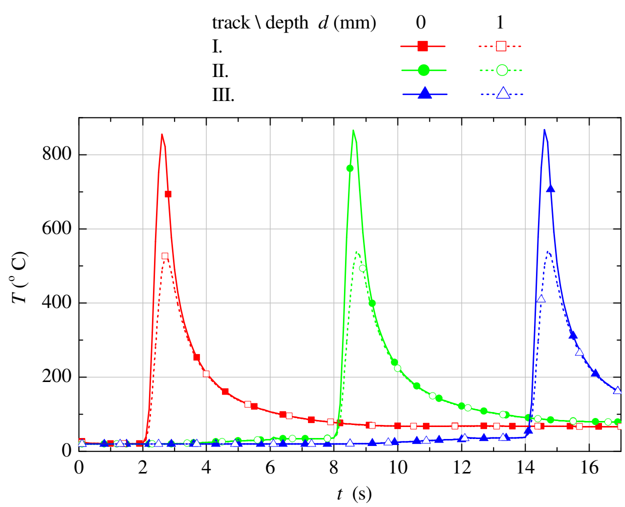

Fig. 9. Time courses of the temperature in the center of tracks I–III at the surface and the depth of 1 mm ($x = 50$ mm).

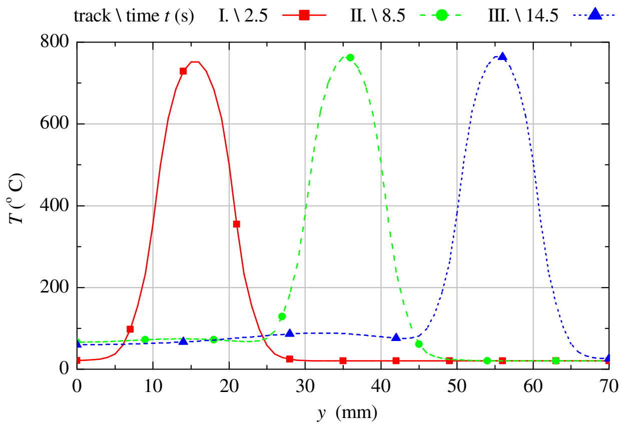

Fig. 10. Spatial courses in the y-axis direction passing the center of the sample front surface ($x = 50$ mm, $z = 0$ mm) for the times when the laser is over the center of each track.

D. Sample Temperature Distribution and the Possibilities of Depth Evaluation of Laser Treatment

Figure 11 gives the image of spatial temperature distribution in the sample that undergoes thermal treatment using a moving laser beam. The figure shows the temperature state at the time 2.5 [Fig. 11(a)] and 17.5 s [Fig. 11(b)], when the laser beam is over the center of the track during the first and fourth movement. The maximum surface temperatures are 874°C and 964°C, respectively, on the heat-loaded sample surface. Transversal cross sections passing the sample center, Fig. 11 ($x = 50$ mm), indicate the shape of the heat-affected zone in the sample. Beam motion velocity 24 $\text{mm} \cdot \text{s}^{-1}$ is considered in the simulation.

These temperature data can be further processed in order to evaluate the maximum temperature $T_{\max}(x, y, z)$ at each sample position (x, y, z) during the entire laser treatment process:

$$T_{\max}(x, y, z) = \max\{T(x, y, z); t \in \langle t_i, t_f \rangle\}, \tag{21}$$

where t_i, $t_f(s)$ are the initial and final times of the process. Taking the hardening temperature T_h(Subsection 2.A), the

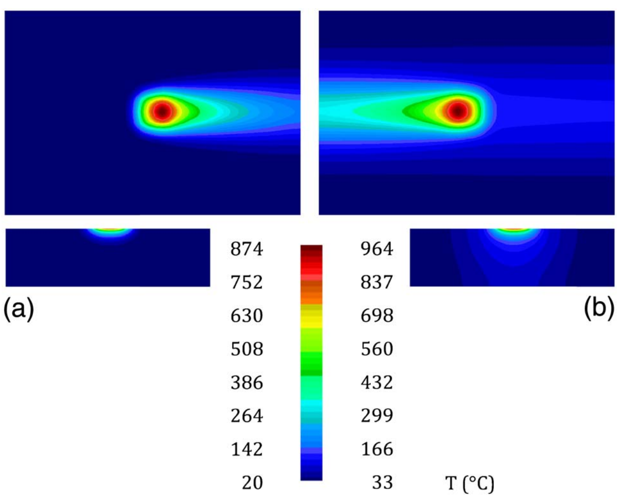

Fig. 11. Distribution of the temperature at the sample front surface and at transversal sample cross sections when the heat source is in the center of the track during the (a) first and (b) fourth movements.

Table 2. Multiple Movements across the Same Track[a]

No. of Movements/ Distance from Track (mm)	0	1	2
1	0.167	0.076	0
2	0.302	0.227	0.070
3	0.378	0.305	0.154
4	0.434	0.364	0.217

[a]The depths of hardening d_n(mm) reached in the track and at the perpendicular distance of 1 and 2 mm from the track.

Table 3. One Movement across Multiple Tracks[a]

No. of Tracks/Distance from Track (mm)	0
I	0.168
II	0.201
III	0.207

[a]The depths of hardening d_n(mm) reached in the center of individual tracks.

region of the material where the laser hardening has been performed can be defined by the equation

$$T_{\max}(x, y, z) \geq T_h. \tag{22}$$

The depth of hardening d_h is the thickness of the laser hardening region and can be defined as

$$d_h(x, y) = z, \quad \text{where} \quad T_{\max}(x, y, z) = T_h. \tag{23}$$

The cases of multiple movements across the same track and one movement across multiple tracks have been selected for evaluation of the depths of hardening. The hardening depth d_h, dependent on the distance from the laser track in the case of multiple movements, can be observed in Table 2. The evaluation is done in the y-axis direction from the center of the sample surface ($x = 50$ mm) for positions that are 0, 1, and 2 mm from the track. For positions that are farther than 2 mm, the number of laser movements necessary for hardening of a small subsurface layer increases. The depths of hardening from 0.2 or 0.3 mm are used for real ordinary applications. In the results from the simulation model, the hardening depth of 0.3 mm is achieved in the laser track (0 mm from the laser track) after the second laser movement. Considering the third laser movement, a hardening depth of 0.3 mm is obtained at the position 1 mm from the track. Commercial laser hardening is performed at slower velocities of about 10 $\text{mm} \cdot \text{s}^{-1}$, approximately; thus the depth of hardening in the laser track can reach 1 mm and the hardening depth of 0.3 mm can be found several millimeters from the laser track.

Table 3 is evaluated from the simulation of one movement across multiple tracks; only the positions on the tracks are presented. A small hardening depth of about 0.2 mm is achieved on laser tracks II and III. In the case of real hardening with slower laser motion velocity, the laser-treated zone gets both deeper into the sample material and further from the laser tracks.

4. CONCLUSIONS

The established three-dimensional model of sample heat transfer during surface heat treatment using a moving laser represents an advantageous method for temperature distribution prediction during surface heat treatment. The great benefit of the simulation model is the consideration of the complex boundary conditions of moving laser beam heating. Important effects, such as the spatial non-homogeneous profile of the laser beam, arbitrary laser motion velocity, laser axis position outside the sample, and utilization of multiple laser tracks over the sample have been involved in the model.

The unique contributions of this simulation model include: (1) it is one of the few works published where general energy distribution in the laser beam is utilized, and (2) it is the only work that uses general energy distribution for the simulation model created using commercial computational software. (3) There is no intention to develop a new computational system, but to maximize the use of existing commercial ones. To these commercial computational systems, new procedures for the preparation of non-standard processes, such as heating of material by moving the laser beam, are added. (4) No symmetry of the sample is assumed; the full geometry of the sample is simulated. (5) Real thermal losses of the sample to the surroundings are considered. (6) In this model, there is the possibility to take into account the irregular velocity of the laser beam during its tracking over the sample.

Using the simulation model, three cases of heat treatment have been used for presentation of both model utilization and simulation results.

The motion velocity and number of beam movements over the sample have been confirmed as important factors influencing the results achieved. Lowering the beam motion velocity from 40 $\mathrm{mm \cdot s^{-1}}$ to 24 and 17.14 $\mathrm{mm \cdot s^{-1}}$, the sample surface maximum temperature increases from 700°C to 877°C and 1005°C during the first beam movement over the sample. During a second beam movement, the sample surface maximum temperature increases from 744°C to 920°C and 1049°C.

Multiple laser beam movements across the sample utilizing the same track have been presented for up to four laser beam movements. During the first movement of the laser beam over the sample, the sample temperature at the center of the track reaches over 800°C. Increasing the number of movements, this temperature slightly increases to nearly 950°C during the fourth movement. The trends of sample temperature dependence on the distance from the laser track in the y- and z-axes directions have been discussed.

Utilization of multiple laser tracks with one movement above them has been illustrated by using three parallel tracks in the x-axis direction. The peak values of sample surface temperature in the y-axis direction approached approximately 870°C in the laser tracks.

The great power of the established simulation model lies in the possibility of prediction of sample maximum temperatures during the entire heat treatment process. Using maximum temperature evaluation, the isotherm surfaces in the sample volume can be constructed. When a temperature value of the isotherm is set to the laser hardening temperature, the appropriate isotherm would predict the laser hardening region in the sample.

Using the established simulation model, it is possible to investigate the effect of process parameters (laser beam motion velocity, heat source power, thermal properties of processed material, etc.), or to perform process optimization without the necessity of doing a series of experiments.

Funding. Ministerstvo Školství, Mládeže a Tělovýchovy (MŠMT).

Acknowledgment. The result was developed within the CENTEM project, reg. no. CZ.1.05/2.1.00/03.0088, cofunded by the ERDF as part of the Ministry of Education, Youth and Sports OP RDI programme and, in the follow-up sustainability stage, supported through CENTEM PLUS (LO1402) by financial means from the Ministry of Education, Youth and Sports under the "National Sustainability Programme."

REFERENCES

1. Z. B. Hou and R. Komanduri, "General solutions for stationary/moving plane heat source problems in manufacturing and tribology," Int. J. Heat Mass Transfer **43**, 1679–1698 (2000).
2. P. Levin, "A general solution of 3-D quasi-steady-state problem of a moving heat source on a semi-infinite solid," Mech. Res. Commun. **35**, 151–157 (2008).
3. S. Liu, S. Lannon, Q. Wang, and L. Keer, "Solutions for temperature rise in stationary/moving bodies caused by surface heating with surface convection," J. Heat Transfer **126**, 776–785 (2004).
4. Ch.-K. Kim, "An analytical solution to heat conduction with a moving heat source," J. Mech. Sci. Technol. **25**, 895–899 (2011).
5. N. Bianco, O. Manca, S. Nardini, and S. Tamburino, "Transient heat conduction in solids irradiated by a moving heat source," Defect Diffus. Forum **283–286**, 358–363 (2009).
6. S. Saedodin, M. Akbari, A. Raisi, and M. Torabi, "Calculation and investigation of temperature distribution and melt pool size due to a moving laser heat source using the solution of hyperbolic heat transfer equation," World Appl. Sci. J. **11**, 1273–1281 (2010).
7. I. B. Ivanovic, A. S. Sedmak, M. V. Miloš, A. B. Živkovic, and M. M. Lazic, "Numerical study of transient three-dimensional heat conduction problem with a moving heat source," Therm. Sci. **15**, 257–266 (2011).
8. H. Boffy, M.-Ch. Baietto, P. Sainsot, and A. A. Lubrecht, "Detailed modeling of a moving heat source using multigrid methods," Tribol. Int. **46**, 279–287 (2012).
9. Ch.-K. Kim, "Adaptive finite element solution for the heat conduction with a moving heat source," J. Mech. Sci. Technol. **26**, 967–972 (2012).
10. M. Akbari, D. Sinton, and M. Bahrami, "Geometrical effects on the temperature distribution in a half-space due to a moving heat source," J. Heat Transfer **133**, 064502 (2011).
11. Z. Zeng, J. M. B. Brown, and A. E. Vardy, "On moving heat sources," Heat Mass Transfer **33**, 41–49 (1997).
12. M. Honner, P. Červený, V. Franta, and F. Čejka, "Heat transfer during HVOF deposition," Surf. Coat. Technol. **106**, 94–99 (1998).
13. Z. Veselý, J. Kuneš, M. Honner, and J. Martan, "TBC dynamic behavior during thermal shocks—simulation and experiment," in *Proceedings of 7th International Conference on Advanced Computational Methods in Heat Transfer*, Halkidiki, Greece (2002), pp. 503–512.
14. Z. Veselý, "Thermomechanical processes in heterogeneous layered structure of thermal barrier coating during thermal shock," (in Czech) Ph.D. thesis (University of West Bohemia, 2002), p. 171.
15. J. Kuneš, Z. Veselý, and M. Honner, Thermal Barriers (in Czech) (Academia, 2003).
16. M. Honner and J. Šroub, "Modeling of thermal spraying heat transfer processes by exodus stochastic method," J. Therm. Spray Technol. **18**, 1014–1021 (2009).
17. J. Mach, "Modeling of thermal processes during surface laser treatment of steel," (in Czech) Diploma thesis (University of West Bohemia, 2007), p. 79.

18. Z. Veselý, M. Honner, and J. Mach, "2D and 3D unsteady simulation of the heat transfer in the sample during heat treatment by moving heat source," World Acad. Sci. Eng. Technol. **9**, 1778–1783 (2015).
19. V. A. Serebryakov, K. V. Gratsianov, A. S. Eremenko, A. A. Timofeev, M. V. Volkov, and S. Zou, "Laser strengthening of metals," J. Opt. Technol. **72**, 237–240 (2005).
20. J. Yang, Y. Hua, R. Chen, L. Cai, Y. Zhang, and H. Yan, "Microstructure and properties of plastic deformed martensite induced by laser shock processing," Chin. Opt. Lett. **2**, 715–717 (2004).
21. L. Li, "The advances and characteristics of high-power diode laser materials processing," Opt. Lasers Eng. **34**, 231–253 (2000).
22. F. Bachmann, P. Loosen, and R. Poprawe, *High Power Diode Lasers: Technology and Applications* (Springer, 2007).
23. J. C. Ion, "Laser transformation hardening," Surf. Eng. **18**, 14–31 (2002).
24. S. Martínez, A. Lamikiz, I. Tabernero, and E. Ukar, "Laser hardening process with 2D scanning optics," Phys. Procedia **39**, 309–317 (2012).
25. M. Hruška, M. Vostřák, E. Smazalová, and M. Švantner, "Standard and scanning laser hardening procedure," in *Proceedings of the 22nd International Conference on Metallurgy and Materials*, Brno, Czech Republic (2013), pp. 1–6.
26. M. Hruška, M. Vostřák, E. Smazalová, and M. Švantner, "3D scanning laser hardening," in *Proceedings of the 23rd International Conference on Metallurgy and Materials*, Brno, Czech Republic (2014), pp. 1–6.
27. E. Kennedy, G. Byrne, and D. N. Collins, "A review of the use of high power diode lasers in surface hardening," J. Mater. Process. Technol. **155–156**, 1855–1860 (2004).

Queries

1. AU: The funding information for this article has been generated using the information you provided to OSA at the time of article submission. Please check it carefully. If any information needs to be corrected or added, please provide the full name of the funding
798 organization/institution as provided in the CrossRef Open Funder Registry (http://www.crossref.org/fundingdata/registry.html).

2. AU: A check of online databases found a different year for this reference. Please check that this is the reference you intended to cite.